



**HAL**  
open science

# Unexpected Formation of the Iodobismuthate Salt $(C_{14}H_{15}S_2N_2)_2(C_9H_{10}SN)_2[Bi_4I_{16}]$ upon Reaction of the Unsaturated Ligand Z-PySCH<sub>2</sub>CH=CHCH<sub>2</sub>SPy with BiI<sub>3</sub>

Marwa Essid, Chakib Hrizi, Salah Ammar, Abderrahim Khatyr, Michael Knorr, Annika Schmidt, Carsten Strohmann

## ► To cite this version:

Marwa Essid, Chakib Hrizi, Salah Ammar, Abderrahim Khatyr, Michael Knorr, et al.. Unexpected Formation of the Iodobismuthate Salt  $(C_{14}H_{15}S_2N_2)_2(C_9H_{10}SN)_2[Bi_4I_{16}]$  upon Reaction of the Unsaturated Ligand Z-PySCH<sub>2</sub>CH=CHCH<sub>2</sub>SPy with BiI<sub>3</sub>. Molbank, 2023, 2024 (1), pp.M1755. 10.3390/M1755 . hal-04410596

**HAL Id: hal-04410596**

**<https://hal.science/hal-04410596v1>**



Submitted on 14 Oct 2024

**HAL** is a multi-disciplinary open access archive for the deposit and dissemination of scientific research documents, whether they are published or not. The documents may come from teaching and research institutions in France or abroad, or from public or private research centers.

L'archive ouverte pluridisciplinaire **HAL**, est destinée au dépôt et à la diffusion de documents scientifiques de niveau recherche, publiés ou non, émanant des établissements d'enseignement et de recherche français ou étrangers, des laboratoires publics ou privés.

Communication

# Unexpected Formation of the Iodobismuthate Salt $(C_{14}H_{15}S_2N_2)_2(C_9H_{10}SN)_2[Bi_4I_{16}]$ upon Reaction of the Unsaturated Ligand Z-PySCH<sub>2</sub>CH=CHCH<sub>2</sub>SPy with BiI<sub>3</sub>

Marwa Essid<sup>1</sup>, Chakib Hrizi<sup>1,\*</sup>, Salah Ammar<sup>1</sup>, Abderrahim Khatyr<sup>2</sup>, Michael Knorr<sup>2,\*</sup>, Annika Schmidt<sup>3</sup> and Carsten Strohmann<sup>3</sup>

- <sup>1</sup> Unité de recherche Electrochimie, Matériaux et Environnement (UR17ES45), Faculté des Sciences de Gabès, Université de Gabès, Cité Erriadh, Gabès 6072, Tunisia; essid.marwa@yahoo.com (M.E.); salah.ammar@fsg.rnu.tn (S.A.)
- <sup>2</sup> Institut UTINAM UMR 6213 CNRS, Université de Franche-Comté, 16, Route de Gray, 25030 Besançon, France; abderrahim.khatyr@univ-fcomte.fr
- <sup>3</sup> Anorganische Chemie, Technische Universität Dortmund, Otto-Hahn Straße 6, 44227 Dortmund, Germany; annika5.schmidt@tu-dortmund.de (A.S.); carsten.strohmamm@tu-dortmund.de (C.S.)
- \* Correspondence: chakib.hrizi@fsg.rnu.tn (C.H.); michael.knorr@univ-fcomte.fr (M.K.); Tel.: +33-3-81-66-62-70 (M.K.)

**Abstract:** The olefinic dithioether (Z)-1,4-bis(pyridin-2-ylthio)but-2-ene Z-PyS(CH<sub>2</sub>CH=CHCH<sub>2</sub>)SPy (L) was prepared by the treatment of *cis*-ClCH<sub>2</sub>CH=CHCH<sub>2</sub>Cl with in situ generated potassium pyridine-2-thiolate Py-SK and analyzed by IR and NMR spectroscopy. To investigate the chemistry of polynuclear iodobismuthate complexes, two equivalents of BiI<sub>3</sub> were reacted with L in the MeOH solution to afford the anionic tetranuclear title compound  $(C_{14}H_{15}S_2N_2)_2(C_9H_{10}SN)_2[Bi_4I_{16}]$  with a *N*-protonated (Z)-1,4-bis(pyridin-2-ylthio)but-2-ene as a counterion. Compound **1** was characterized by IR and UV spectroscopy; the formation of a tetranuclear framework was ascertained by a single-crystal X-ray diffraction study performed at 100 K. Furthermore, an unusual Bi(III)-mediated cyclization of one Z-PyS(CH<sub>2</sub>CH=CHCH<sub>2</sub>)SPy ligand occurred, affording the bicyclic pyridinium salt 3-vinyl-2,3-dihydrothiazolo[3,2-*a*]pyridinium bearing a terminal vinyl group, compensating the second negative charge of the  $Bi_4I_{16}^{4-}$  cluster anion. The SCXRD characterization was completed by a Hirshfeld surface analysis, revealing some secondary interactions occurring in the crystal.

**Keywords:** bismuth triiodide; olefinic dithioether; crystal structure; Hirshfeld analysis



**Citation:** Essid, M.; Hrizi, C.; Ammar, S.; Khatyr, A.; Knorr, M.; Schmidt, A.; Strohmamm, C. Unexpected Formation of the Iodobismuthate Salt  $(C_{14}H_{15}S_2N_2)_2(C_9H_{10}SN)_2[Bi_4I_{16}]$  upon Reaction of the Unsaturated Ligand Z-PySCH<sub>2</sub>CH=CHCH<sub>2</sub>SPy with BiI<sub>3</sub>. *Molbank* **2024**, *2024*, M1755. <https://doi.org/10.3390/M1755>

Academic Editor: René T. Boéré

Received: 25 November 2023

Revised: 26 December 2023

Accepted: 27 December 2023

Published: 29 December 2023



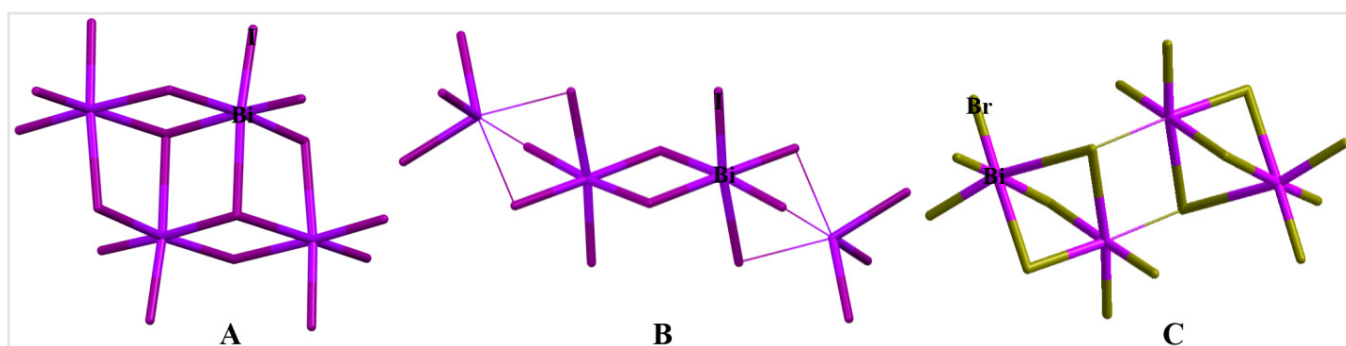
**Copyright:** © 2023 by the authors. Licensee MDPI, Basel, Switzerland. This article is an open access article distributed under the terms and conditions of the Creative Commons Attribution (CC BY) license (<https://creativecommons.org/licenses/by/4.0/>).

## 1. Introduction

The family of trivalent p-block metal halides hybrids, in particular, halogenobismuthates described by the general formula  $Bi_bX_{(3b+a)}R_a$  (where R = organic and X = Cl, Br, and I), have attracted attention as promising low-cost materials, not only due to their non-toxicity and air stability but also due to their interesting optical and electronic properties, including luminescence, semiconductivity, photochromism, thermochromism, etc., [1–4], as well as their fascinating structural topologies. Iodobismuthates hybrid materials have developed over the past few decades due to their electronic properties, optical properties, and diverse structures. Until now, more than 30 different anionic structure types have been structurally characterized [3,5,6]. It has been demonstrated that the anionic inorganic subnetwork ranges from systems based on isolated 0D units (simple anions in  $[BiI_6]^{3-}$ ) to polynuclear cluster motifs such as  $[Bi_8I_{30}]^{6-}$  [4,7–10], through 1D extended chains, most commonly encountered in  $[BiI_4]^-_n$  and  $[BiI_5]^{2-}_n$  [11–13]. To the best of our knowledge, hybrid iodobismuthates featuring a two-dimensional (2D) network are very rare, since just one 2D polymeric structure, namely  $[Bi_{2/3}I_4]^{2-}_n$ , has been reported so far [14].

In the literature, there are three structural types of tetranuclear anions  $\{Bi_4X_{16}\}$ , which we will name  $\alpha$ - $[Bi_4I_{16}]^{4-}$ ,  $\beta$ - $[Bi_4I_{16}]^{4-}$ , and  $\gamma$ - $[Bi_4Br_{16}]^{4-}$  (see Scheme 1). The most fre-

quently used one is  $\alpha$ -[Bi<sub>4</sub>I<sub>16</sub>]<sup>4-</sup>, **A**. It can be described as two sets of edge-sharing [Bi<sub>2</sub>I<sub>10</sub>]<sup>4-</sup> bioctahedra, which are linked through four  $\mu_2$ -I and  $\mu_3$ -I bridges. The  $\alpha$ -[Bi<sub>4</sub>I<sub>16</sub>]<sup>4-</sup> architectures are very common in the literature [15–17], and they also appear for chloride [18] and bromide [19] bismuthates. The second isomer of the {Bi<sub>4</sub>I<sub>16</sub>} anionic family is  $\beta$ -[Bi<sub>4</sub>I<sub>16</sub>]<sup>4-</sup> **B**. It can be represented as containing [Bi<sub>2</sub>I<sub>10</sub>]<sup>4-</sup> anion face shared through six  $\mu_2$ -I atoms with two neutral BiI<sub>3</sub> units. This motif has been reported exclusively for iodides [20,21]. A literature survey shows that a third isomer of Bi<sub>4</sub>X<sub>16</sub> units,  $\gamma$ -[Bi<sub>4</sub>X<sub>16</sub>]<sup>4-</sup>, has been investigated only in bromides [22]. As highlighted in **C**, the rarest isomer  $\gamma$ -[Bi<sub>4</sub>Br<sub>16</sub>]<sup>4-</sup> can be described as a result of the fusion of two binuclear [Bi<sub>2</sub>Br<sub>9</sub>]<sup>3-</sup> moieties in which two  $\mu_2$ -bridging bromide ligands are converted to  $\mu_3$  ones.



**Scheme 1.** Common structural motifs of  $\alpha$ -[Bi<sub>4</sub>I<sub>16</sub>]<sup>4-</sup> (**A**),  $\beta$ -[Bi<sub>4</sub>I<sub>16</sub>]<sup>4-</sup> (**B**), and  $\gamma$ -[Bi<sub>4</sub>Br<sub>16</sub>]<sup>4-</sup> (**C**) [16,20,22].

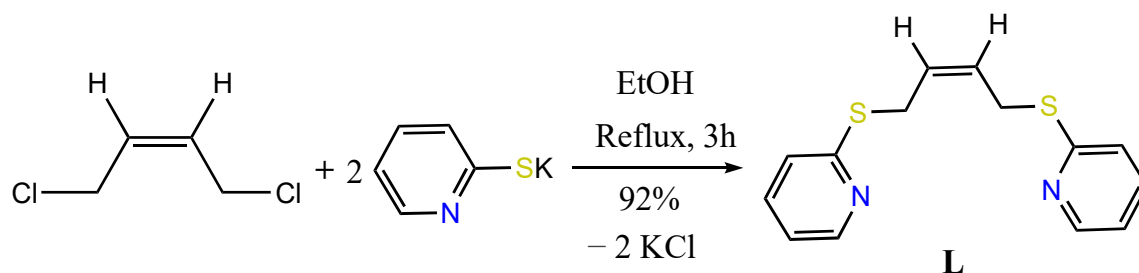
Most halogenobismutates are formed by the addition of hard *N*-donor ligands to the corresponding Bi(III) salts. However, there are also some reports on halogenobismutates obtained by treatment with softer *S*-donor ligands [23,24]. For example, the treatment of BiI<sub>3</sub> with dimethyl sulfide is reported to afford the dinuclear salt [SMe<sub>2</sub>]<sub>2</sub>[Bi<sub>2</sub>I<sub>8</sub>(SMe<sub>2</sub>)<sub>2</sub>] [24]. We recently investigated the reactivity of BiI<sub>3</sub> vis à vis a thione-type ligand [25].

We have described in the past the complexation of unsaturated *Z*-ArS(CH<sub>2</sub>CH=CHCH<sub>2</sub>)SAr on CuX salts, yielding both molecular compounds and coordination polymers (CPs) of type [Cu<sub>4</sub>( $\mu_3$ -I)<sub>4</sub>( $\mu$ -*Z*-ArS(CH<sub>2</sub>CH=CHCH<sub>2</sub>)SAr)<sub>2</sub>]<sub>n</sub> featuring tetranuclear Cu<sub>4</sub>I<sub>4</sub> clusters as secondary building units [26]. In 2004, the isomeric dithioether ligand *E*-PyS(CH<sub>2</sub>CH=CHCH<sub>2</sub>)SPy was prepared by Zheng et al. and reacted with various Ag(I) salts, affording CPs of type [Ag{ $\mu$ -*E*-PyS(CH<sub>2</sub>CH=CHCH<sub>2</sub>)SPy}](NO<sub>3</sub>)<sub>n</sub> [27]. We were therefore intrigued by the outcome using a ligand system featuring a mixed *S,N*-donor set that may lead to a CP of type [(BiI<sub>3</sub>)<sub>n</sub>{ $\mu$ -*E*-PyS(CH<sub>2</sub>CH=CHCH<sub>2</sub>)SPy}] with dative *N*- or *S*-coordination bonds. An example of an *N*-bound coordination polymer is 1D [(Bi<sub>2</sub>I<sub>6</sub>)( $\mu$ -bipy)]<sub>n</sub>, obtained by the reaction of BiI<sub>3</sub> with 4,4'-bipyridine [28]. Alternatively, the formation of an iodobismutate salt of the  $\alpha$ -[Bi<sub>4</sub>I<sub>16</sub>]<sup>4-</sup> type, as mentioned above, may occur. As the third alternative, other structural motifs such as [Bi<sub>2</sub>I<sub>8</sub>]<sup>2-</sup> dimers could be expected a priori [29].

We present in this paper the synthesis of the hitherto unknown unsaturated pyridinic dithioether *Z*-PyS(CH<sub>2</sub>CH=CHCH<sub>2</sub>)SPy (**L**), its reactivity with BiI<sub>3</sub>, and the crystal structure of the resulting tetranuclear iodobismuthate organic inorganic hybrid material **1**.

## 2. Results and Discussion

The ligand *Z*-Py-S(CH<sub>2</sub>CH=CHCH<sub>2</sub>)S-Py (**L**) was synthesized by in situ deprotonation of the aromatic thiol Py-SH in the presence of KOH in an ethanolic solution and subsequent reaction of the thiolate with *cis*-ClCH<sub>2</sub>CH=CHCH<sub>2</sub>Cl, according to Scheme 2. It was isolated in the form of a colorless oil.



**Scheme 2.** Synthesis of the ligand **L**.

The assignment of the internal vibrational modes is based on the comparison with the well-documented spectra of homologous compounds [26,27]. The IR spectrum of **L** in dichloromethane, shown in Figure S2, reveals at high wavenumbers the signals of the aromatic  $\nu(\text{C-H})$  vibrations at 3074, 3048, and 2980  $\text{cm}^{-1}$ . The band located at 2932  $\text{cm}^{-1}$  is associated with the aliphatic  $\nu(\text{C-H})$  vibrations. The absorptions observed at 1580 and 1557  $\text{cm}^{-1}$  are attributed to  $\nu(\text{C}=\text{C})$  and  $\nu(\text{C}=\text{N})$  stretching. In addition, two further absorptions at 1455 and 1415  $\text{cm}^{-1}$  are attributed to the deformation  $\delta(\text{CH}_2)$ . Finally, the bending modes of aromatic  $\delta(\text{C-H})$  appear at 1148 and 1124  $\text{cm}^{-1}$ , while aliphatic  $\delta(\text{C-H})$  bending is detected in the region 1089–986  $\text{cm}^{-1}$ .

Its  $^1\text{H-NMR}$  spectrum in  $\text{CDCl}_3$  (Figure 1) displays a pseudo-quadruplet-like multiplet at  $\delta$  3.96 ppm, attributed to the  $(\text{SCH}_2)$  groups, and the central olefinic  $\text{HC}=\text{CH}$  unit gives rise to a multiplet centered at  $\delta$  5.67 ppm. The simulated spectrum using ChemDraw at 400.1 MHz in  $\text{CDCl}_3$  matches well with the experimental spectrum (Figure S3). Note that the multiplicity of the signals cannot be interpreted by the first order, and the simulated coupling constants are also listed in the supporting material. In the proton-decoupled  $^{13}\text{C-NMR}$  spectrum depicted in Figure 2, the methylene groups and olefinic carbons resonate at 26.8 and 128 ppm, respectively. The assignment of the resonances is based on a comparison with the spectra of related unsaturated compounds *E*-PyS( $\text{CH}_2\text{CH}=\text{CHCH}_2$ )SPy and *Z*-ArS( $\text{CH}_2\text{CH}=\text{CHCH}_2$ )SAr [26,27].

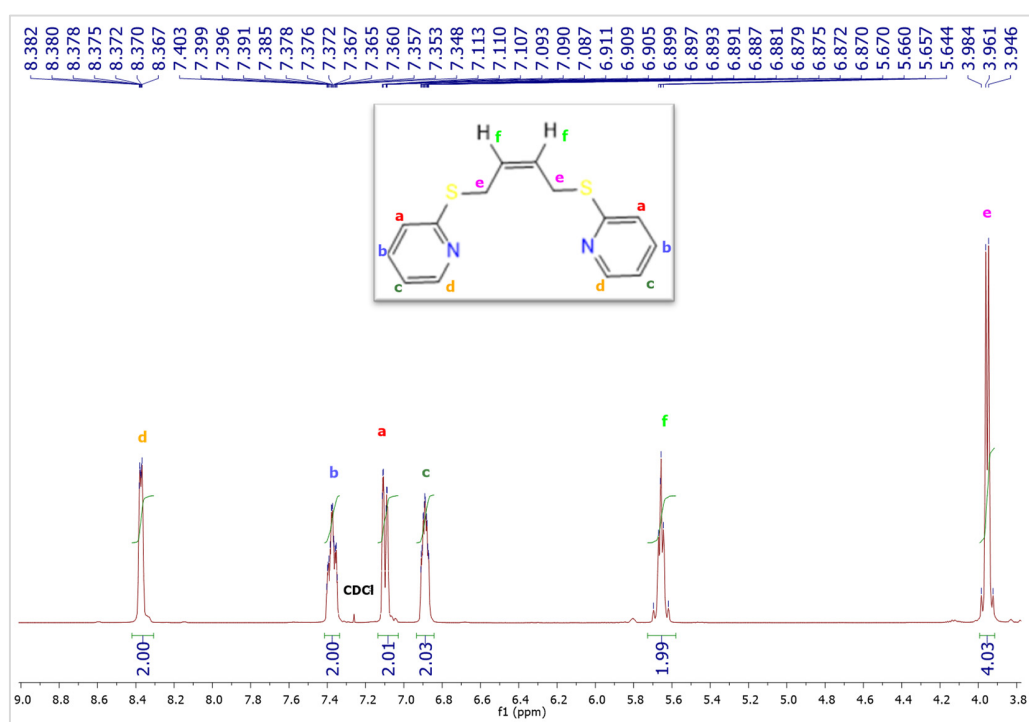


**Figure 1.**  $^1\text{H-NMR}$  spectrum (400.1 MHz,  $\text{CDCl}_3$ ) of **L** at 298 K.

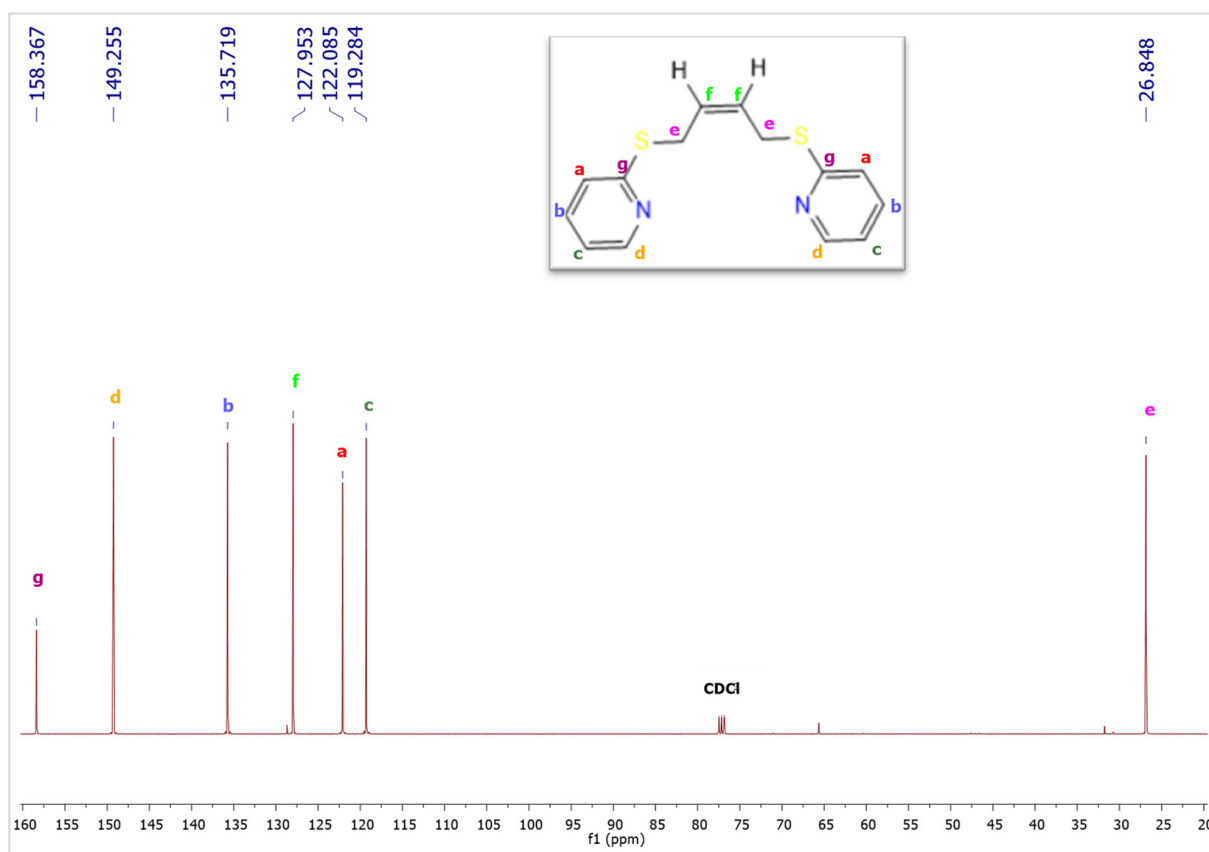
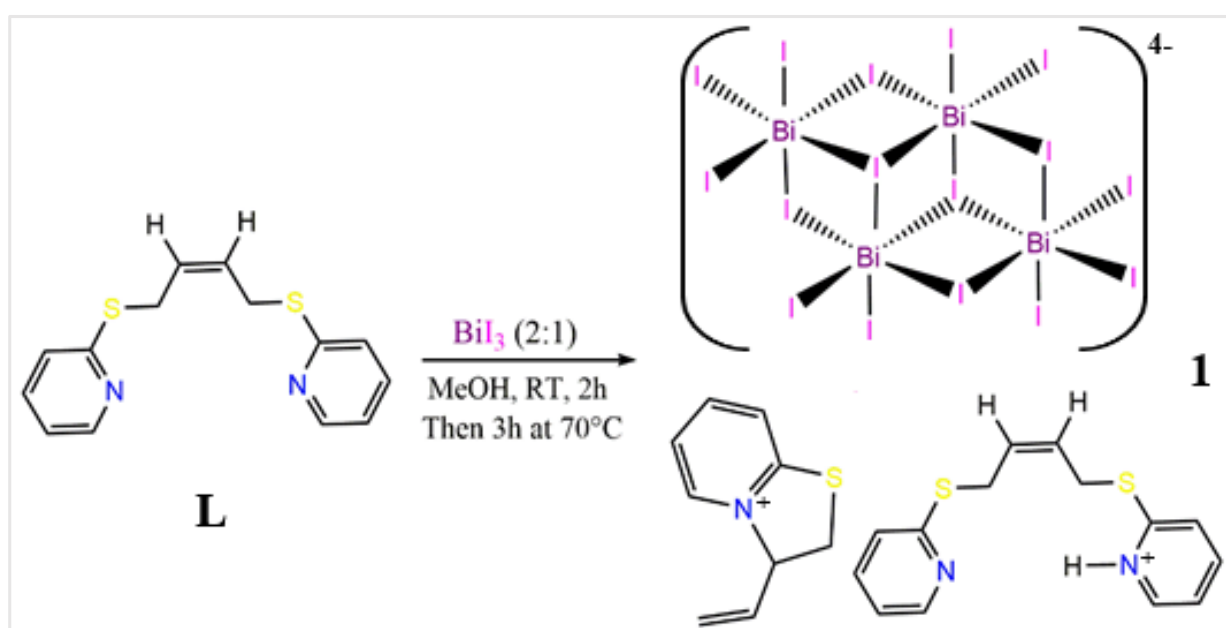


**Figure 2.**  $^{13}\text{C}\{^1\text{H}\}$ -NMR spectrum (100.61 MHz,  $\text{CDCl}_3$ ) of **L** at 298 K.

The title compound **1** was obtained via treatment of  $\text{BiI}_3$  with **L** in a 2:1 molar ratio in a MeOH solution. The reaction was first stirred at room temperature for 2 h, and then heated to  $70^\circ\text{C}$  for 3 h. Upon cooling, the orange solid of **1** was collected by filtration, and the solvent was allowed to evaporate partially to yield air-stable orange crystals (Scheme 3).



**Scheme 3.** Synthesis of the title compound **1**.

As revealed by a single-crystal X-ray diffraction analysis, the tetranuclear compound **1** crystallizes in the monoclinic space group  $P2_1/n$ . As shown in Figure 3, the asymmetric unit of **1** contains half of a  $[\text{Bi}_4\text{I}_{16}]^{4-}$  anion, located on an inversion center, and two different monoprotonated cations, 1,4-bis(pyridinium-2-ylthio)but-2-ene and 3-vinyl-2,3-dihydrothiazolo[3,2-*a*]pyridinium. In fact, the tetranuclear  $[\text{Bi}_4\text{I}_{16}]^{4-}$  is generated from an inversion center via  $\text{Bi}2\text{-I}6\text{-Bi}1^1$  and  $\text{Bi}1^1\text{-I}7\text{-Bi}2^1$  bridges [ $^11-x, 1-y, 2-z$ ] to build the complex  $(\text{C}_{14}\text{H}_{15}\text{S}_2\text{N}_2^+)_2(\text{C}_9\text{H}_{10}\text{SN}^+)_2[\text{Bi}_4\text{I}_{16}^{4-}]$ . Thermal ellipsoid plots of the components of **1** are shown in Figure 3. The zero-dimensional tetraanion is constituted of four distorted  $\text{BiI}_6$  octahedra, which are interconnected in an edge-sharing arrangement. The overall connectivity consists of two sets of edge-sharing dioctahedra mutually sharing three edges to generate the centrosymmetric anion (Figure 3). These specific connectivities of the octahedra give rise to three iodide ligand bonding environments: two  $\mu_3\text{-I}$  (average  $\text{Bi}\text{-}\mu_3\text{-I} = 3.347 \text{ \AA}$ ), four  $\mu_2\text{-I}$  (average  $\text{Bi}\text{-}\mu_2\text{-I} = 3.183 \text{ \AA}$ ), and ten terminal iodides (average  $\text{Bi}\text{-I}_{\text{terminal}} = 2.922 \text{ \AA}$ ). The  $\text{I}\text{-Bi}\text{-I}$  bond angles vary from  $82.194(9)^\circ$  to  $100.147(10)^\circ$  for *cis* and  $168.466(11)^\circ$  to  $177.596(11)^\circ$  for *trans* arrangements. The average intra-ionic  $\text{Bi}\cdots\text{Bi}$  distance in the  $[\text{Bi}_4\text{I}_{16}]^{4-}$  cluster is  $4.874 \text{ \AA}$ . This value is longer than twice the van der Waals radii of Bismuth ( $4.68 \text{ \AA}$ ) [30] and is well in accordance with those found in [1,2-diethyl-3,4,5-trimethyl-pyrazolium] $_4[\text{Bi}_4\text{I}_{16}]$  [31] and  $(\text{H}_2\text{TMDP})_2(\text{Bi}_4\text{I}_{16})\cdot 2\text{EtOH}$  (TMDP = 1,3-bis-(4-piperidyl)propane) [30]. The geometrical features of the  $[\text{Bi}_4\text{I}_{16}]^{4-}$  entities are consistent with those observed in related iodobismuthate compounds [15,31–33]. The distorted octahedral coordination geometry could be interpreted as the beginning of localization of the lone pairs trans to the  $\text{Bi}\text{-Bi}$  vector and/or a geometric arrangement to minimize the  $\text{Bi}\cdots\text{Bi}$  interaction [4,12]. Note that the  $[\text{Bi}_4\text{I}_{16}]^{4-}$  tetraanion is one of the largest known discrete iodobismuthate polyanions in bismuth iodide chemistry. This statement is based on the analysis of all hybrid iodobismuthate structures available in the CSD (vers. 2023) database, revealing thirty-seven entries for the  $[\text{Bi}_4\text{I}_{16}]^{4-}$  motif. For example, treatment of  $\text{BiI}_3$  with *L*-cysteine in the presence of HI is reported to afford  $[\text{Bi}_4\text{I}_{16}]^{4-}$  clusters, whose negative charge is balanced by two protonated *L*-cysteine $\text{H}_2$  cations [34]. The solvothermal reaction of a mixture of  $\text{BiI}_3$ , the salt 1,1''-(1,4-butanediyl)bis[4,4'-bipyridinium]bis[tetrafluoroborate] (bbpyf) and HI resulted in the formation of a 2D supramolecular consisting of [bbpy][ $\text{Bi}_4\text{I}_{16}$ ] units [35]. Further examples are  $[\text{C}_6\text{H}_{14}\text{N}_2]_2[\text{Bi}_4\text{I}_{16}]\cdot 2\text{H}_2\text{O}$  resulting from solvothermal reaction between  $\text{BiI}_3$ , 1,2-benzenediamine in EtOH [36] or  $(1,3\text{-MePy})_4\{[\text{Bi}_4\text{I}_{16}](\text{I}_2)\}$  stemming from a mixture of  $\text{BiI}_3$ , 1,3-dimethylpyridinium iodide and HI in MeCN solution [37]. Similar tetranuclear  $\alpha$ -type anions  $[\text{Bi}_4\text{X}_{16}]^{4-}$  [5] are described in the literature for  $\text{X} = \text{Cl}$  and  $\text{X} = \text{Br}$  [38,39]. Related iodoantimonate anions of the  $\alpha$ -type,  $[\text{Sb}_4\text{I}_{16}]^{4-}$ , were investigated by Vasiliev et al. [40].

From the dimensional reduction concept, the 1D anion  $\text{Bi(III)I}_4^-$  can be obtained by excision of the 2D layer of the parent  $\text{BiI}_3$  structure by adding an equivalent of  $\text{I}^-$  to  $\text{BiI}_3$  (Scheme S1). By adding another  $\text{I}^-$ , further dimensional reduction in this chain can lead, in turn, to a  $\text{Bi}_2\text{I}_{10}^{4-}$  edge-shared octahedra dimer [41]. Starting from the binuclear  $[\text{Bi}_2\text{I}_{10}]^{4-}$  unit, the tetranuclear  $[\text{Bi}_4\text{I}_{16}]^{4-}$  can be constructed by the hypothetical addition of two neutral  $\text{BiI}_3$  molecules on opposing sides of the previous anion ( $\text{Bi}_2\text{I}_{10}^{4-} + 2 \text{BiI}_3 = \text{Bi}_4\text{I}_{16}^{4-}$  and  $\text{Bi}_4\text{I}_{16}^{4-} + 2 \text{BiI}_3 = \text{Bi}_6\text{I}_{22}^{4-}$ ) (see Scheme S1) [41]. This leads to a connectivity of the octahedra that is also found in the layered  $\text{CdI}_2$  structure [42]. So, the  $[\text{Bi}_4\text{I}_{16}]^{4-}$  anion can also be viewed as a cut-out of those layers.

As shown in Figure 4A, the organic cations  $[\text{C}_{14}\text{H}_{15}\text{S}_2\text{N}_2]^+$  form a dimer by the self-assembly of extensive intermolecular hydrogen bonds ( $\text{N}2\text{-H}2\cdots\text{S}3 = 2.891 \text{ \AA}$ ,  $\text{N}2\text{-H}2\cdots\text{N}3 = 1.813 \text{ \AA}$ ). These distances are much shorter than the sum of the Van Der Waals radii of H and S atoms ( $1.2 + 1.8 = 3 \text{ \AA}$ ) and of H and N atoms ( $1.2 + 1.55 = 2.75 \text{ \AA}$ ). These dimers are in close contact with the  $[\text{C}_9\text{H}_{10}\text{SN}]^+$  cations via  $\text{H/S}\cdots\pi$  interactions (with  $d(\text{H}7\cdots\text{N}3/\text{C}19\text{-C}23) = 2.903 \text{ \AA}$  and  $d(\text{S}1\cdots\text{N}2/\text{C}15\text{-C}17) = 3.716 \text{ \AA}$ ), and very strong hydrogen bonds of type  $\text{H}\cdots\text{N/S}$  are also observed ( $\text{H}7\cdots\text{N}3 = 2.530 \text{ \AA}$  and  $\text{H}6\cdots\text{S}2 = 2.877 \text{ \AA}$ ) (Figure 4B, Table S2), serving to tether them together into a 2D supramolecular layered network (see Figure 5A).

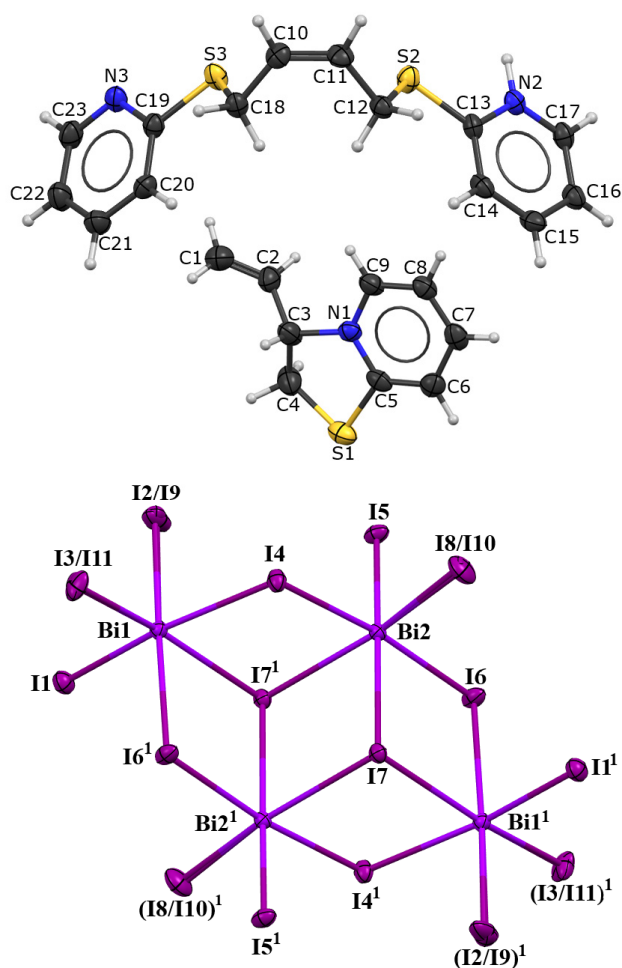


**Figure 3.** Ellipsoid plots of the two cations (**top**) and the complete centrosymmetric  $[\text{Bi}_4\text{I}_{16}]^{4-}$  anion (**bottom**) of **1**. Displacement ellipsoids are drawn at the 50% probability level, and H atoms are small spheres of arbitrary radii. More selected bond lengths and angles are presented in Table S1 of the supporting material ( $^11-x, 1-y, 2-z$ ).

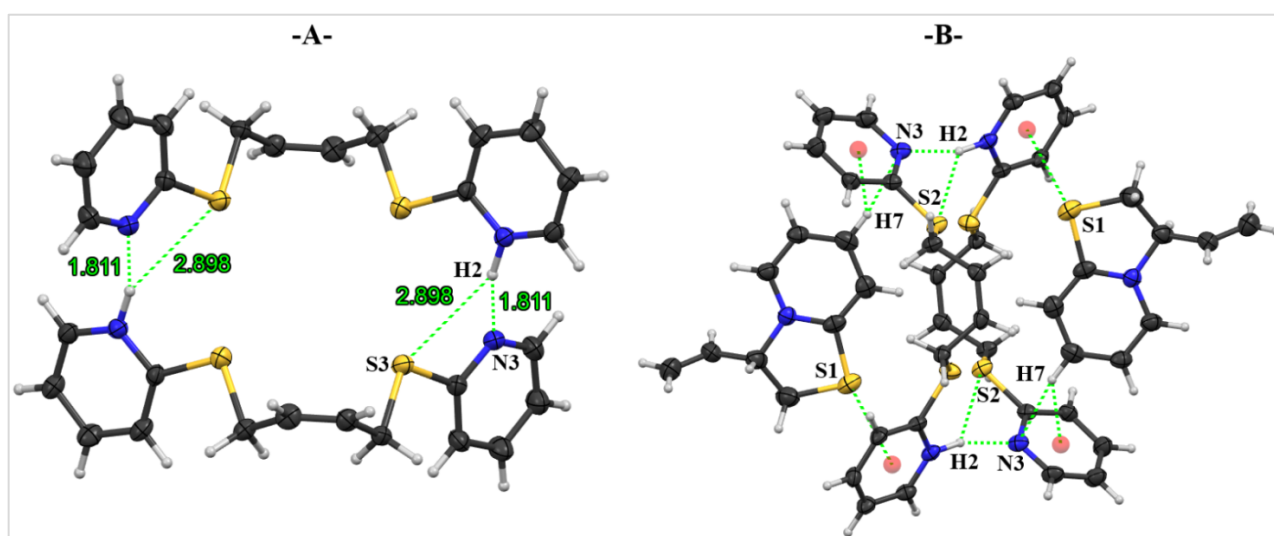


**Figure 4.** Dimers of  $[\text{C}_{14}\text{H}_{15}\text{S}_2\text{N}_2]^+$  cations formed via N-H $\cdots$ N/S intermolecular hydrogen bonds (A), The intermolecular interactions between dimer and  $[\text{C}_9\text{H}_{10}\text{SN}]^+$  cations via numerous H/S $\cdots$  $\pi$  and H $\cdots$ N/S interactions (B).

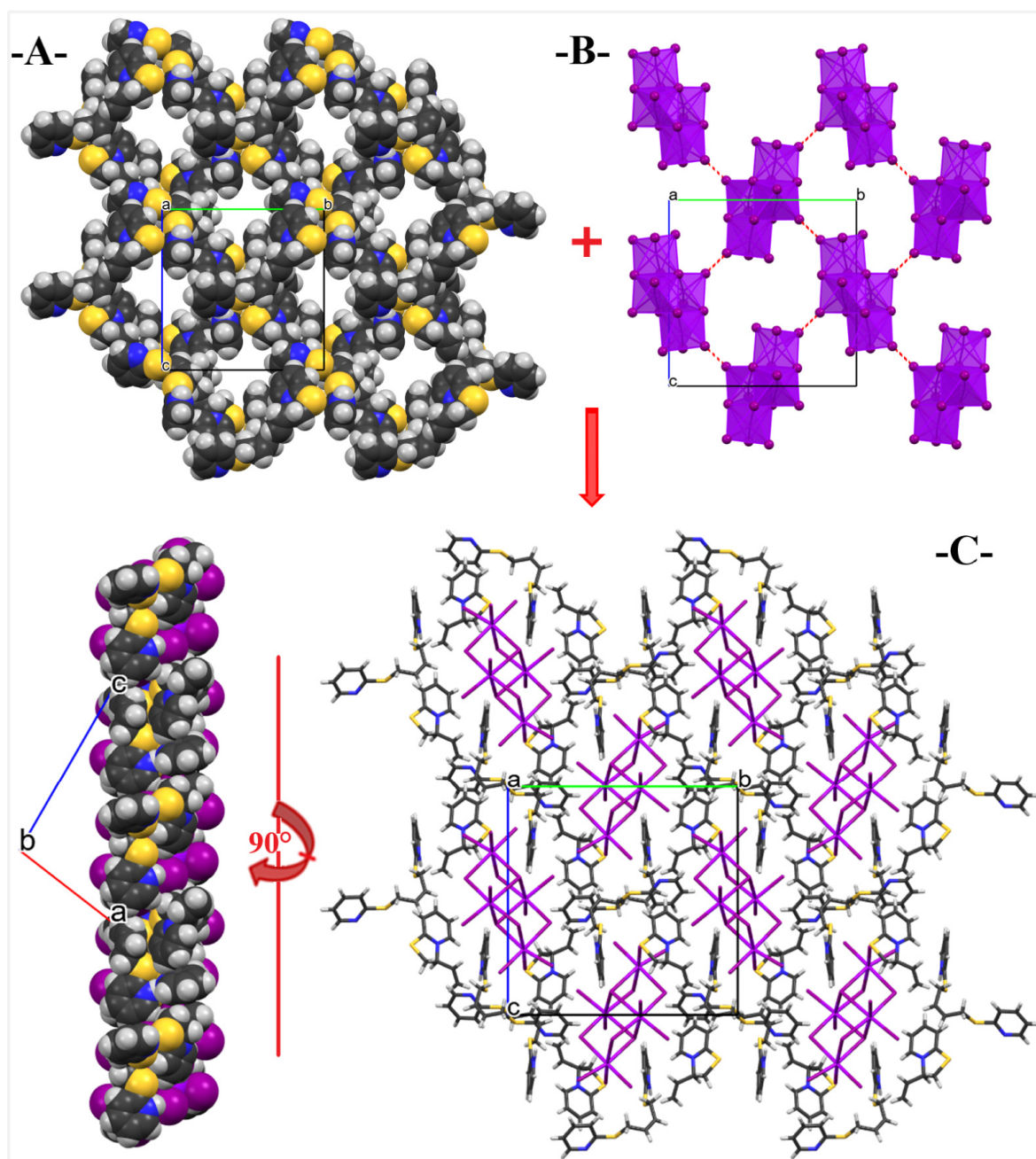


**Figure 5.** Crystal structure of **1**: (A) Space filling representation of the open-2D H-bonded supramolecular network of organic cations; (B) View of pseudo-2D supramolecular layer of  $\{[Bi_4I_{16}]\}$  anions with I...I interactions (highlighted in red); (C) View of the crystal packing along [100], showing the 2D H-bonded supramolecular networks of organic entities, which accommodates  $[Bi_4I_{16}]^{4-}$  anions in windows.

As highlighted in the view along the *a*-axis (Figure 5), the crystal structure of **1** is built from the packing of these open-2D supramolecular layers of organic cations, which accommodate the  $[Bi_4I_{16}]^{4-}$  anions in windows. Each  $[Bi_4I_{16}]^{4-}$  anion forms four I...I contacts with the four nearest anions. The shortest distance between the I atoms is 3.993 Å (I3...I5), which is slightly greater than the sum of the van der Waals radii of two I atoms (3.96 Å). These I...I interactions link the 0D anionic components by extending them along the *b*- and *c*-axis to produce a pseudo-two-dimensional  $\{[Bi_4I_{16}]^{4-}\}$  arrangement, which is stacked perpendicular to the [101] crystallographic direction (see Figures 5A and S5).



When viewing the crystal structure along the *b*-direction (Figures 5C and S7), the pseudo-2D arrangement of the anionic moieties with the 2D supramolecular layer of organic cations forms a sheet in the (202) plan (Figure 5C). A second layer of the 2D supramolecular network is stacked on top or down, perpendicular to the [101] direction (Figure S6). The cohesion between adjacent layers was held by a weak I⋯I halogen bond between the iodide atoms on adjacent sheets with  $d(\text{I8}\cdots\text{I4}) = 4.256 \text{ \AA}$ . This interaction links the adjacent sheets together into a three-dimensional array (which is extended perpendicular to the [101] direction). This distance exceeds the sum of the van der Waals radii of two I atoms ( $3.96 \text{ \AA}$ ) and is much shorter than twice the ionic radius for the iodide ion ( $2.2 \text{ \AA}$ ) [43]. In comparison with crystalline  $\text{I}_2$ , the intermolecular I⋯I distances are  $3.50 \text{ \AA}$  and  $3.97 \text{ \AA}$  (intra-layer), and  $4.27 \text{ \AA}$  between layers [44]. In addition, there are numerous H⋯I interactions (represented on Figure S3) in the range of  $3.062\text{--}3.315 \text{ \AA}$  between each I and H atom of the  $[\text{C}_{14}\text{H}_{15}\text{S}_2\text{N}_2]^+$  and  $[\text{C}_9\text{H}_{10}\text{SN}]^+$  cations (the sum of sum of the Van Der Waals radii of H and I is  $3.18 \text{ \AA}$ ). We clearly see  $[\text{C}_{14}\text{H}_{15}\text{S}_2\text{N}_2]^+$  molecules interacting with terminal and  $\mu_2$ -bridging iodide via short C-H⋯I hydrogen bonding interactions (with  $d(\text{H}\cdots\text{I})$  ranging from  $3.134$  to  $3.315 \text{ \AA}$  for the terminal iodide and from  $3.306$  to  $3.309 \text{ \AA}$  for  $\mu_2$ -I bridging, respectively). The  $[\text{C}_9\text{H}_{10}\text{SN}]^+$  cations are involved in quite strong C4-H4B⋯I4 ( $d(\text{H}\cdots\text{I}) = 3.077 \text{ \AA}$ ) hydrogen bond and in C-H⋯I short contacts with the terminal iodides ( $d(\text{H}\cdots\text{I})$  in the  $3.062\text{--}3.312 \text{ \AA}$  range). Overall, the structure can be viewed as a three-dimensional connected array when all the I⋯I intra/interlayer and hydrogen-bonding interactions are considered.

Furthermore, Hirshfeld molecular surface analyses were performed and generated using the Crystal Explorer 17 program [45,46], allowing the visualization of the different types of interactions within the crystal structure. The normalized contact distances,  $d_{\text{norm}}$ , are charted in the range  $-0.680$  to  $0.981 \text{ a.u.}$ ;  $d_e$  was mapped between (red)  $0.6$  and (blue)  $2.6 \text{ \AA}$ , and Shape Index, *S*, was mapped between  $-1.0$  (red) and  $+1.0$  (blue) (Figure 6). The white surface indicates contacts with distances equal to the sum of van der Waals radii, and the red and blue surfaces indicate distances shorter (in close contact) or longer (distinct contact) than the van der Waals radii, respectively. The presented areas are supportive of the intermolecular interactions described in previous sections.

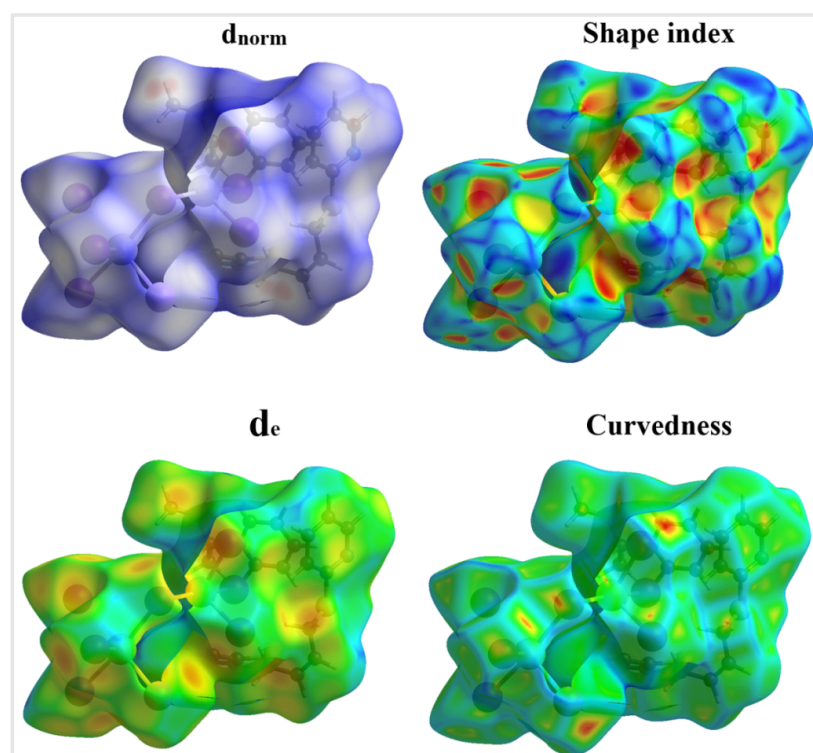


**Figure 6.** Hirshfeld surfaces of **1**, mapped with  $d_{\text{norm}}$ , shape index,  $d_e$ , and curvedness.

The quantitative analysis provided by total and composed fingerprint plots (FPs) of the main intermolecular contacts is shown in Figure 6 with their relative contributions to the Hirshfeld surface. Indeed, the most important interaction is  $H \cdots I/I \cdots H$ , which emerges in a total of 57% of the Hirshfeld surface area, showing that those interactions have the most significant contribution in the supramolecular net (Figure 6). These interactions, supported by a quantitative analysis provided by a 2D fingerprint plot, appear as two symmetrical spikes (where  $d_e > d_i$ ), emphasizing the donor character played by the organic cations. The  $H \cdots H$  interactions appear in the fingerprint plot with an overall HS contribution of 11.3% (Figure 7), which is due to the large number of short  $H \cdots H$  interatomic contacts. These interactions appear as widely scattered points of high density (where  $d_e = d_i = 1.2 \text{ \AA}$ ). The organic cations are involved in significant  $H \cdots \pi/\pi \cdots H$  and  $H \cdots S/S \cdots H$  interactions. These interactions were evaluated by means of Hirshfeld surface analysis mapped according to  $d_{\text{norm}}$ , showing their relative contribution of 5.7% and 5%, respectively, in the totality of interactions percentage (see Figure 7). These interactions appear as widely dispersed high-density points. For anionic units,  $I \cdots I$  interactions were detected with a percentage of 4.3%, helping in the maintenance of the cohesion of the structure. The other interactions, i.e.,  $I \cdots C/C \cdots I$  and  $N \cdots H/H \cdots N$  appear with relatively minor percentages of Hirshfeld surface area (4.9% and 2.4%), respectively.

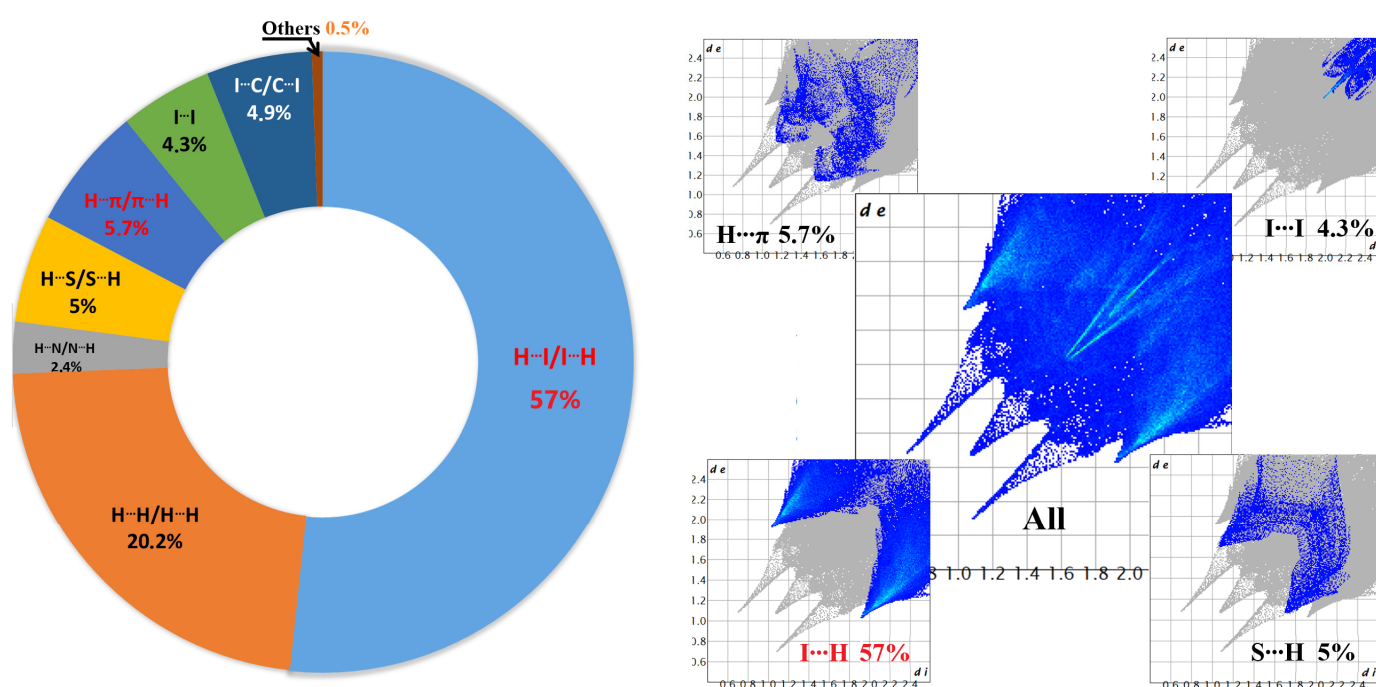


**Figure 7.** Pie graph for compound **1** showing the percentage contribution of the individual atomic contacts to the Hirshfeld surface (left). Highlighting  $I \cdots H$ ,  $S \cdots H$ ,  $H \cdots \pi$ , and  $I \cdots I$  contacts and 2D fingerprint plot in crystal stacking for **1** (right).

### 3. Discussion

While the formation of a higher-nuclear halogenobismuthate cluster upon reaction with *S*- or *N*-donor ligands (see examples cited above) is not uncommon, the protonation of **L** and the cyclization of a second **L** molecule yielding 3-vinyl-2,3-dihydrothiazolo[3,2-*a*]pyridinium salt deserve some comment. The protonation of *N*-donor ligands in polar solvents such as MeCN, THF, or MeOH has also been reported [31,32,47]. For example, the treatment of  $\text{BiI}_3$  with 4,4'-bipyridine in THF affords the iodobismuthate salt  $[4,4'\text{-H}_2\text{bipy}]^{2+}[\text{Bi}_2\text{I}_8(4,4'\text{-bipy})_2]^{2-}$  [47]. More intriguing is the formation of the hitherto unknown salt 3-vinyl-2,3-dihydrothiazolo[3,2-*a*]pyridinium. A similar heterocyclic scaffold, namely 3-ethoxy-2*H*,3*H*-[1,3]thiazolo[3,2-*a*]pyridinium bromide bearing an ethoxy group

at the three-position of the five-membered dihydro-thiazole cycle, has been prepared by treatment of 2-pyridinesulfenyl bromide with vinyl ethyl ether [48]. To rationalize the formation of 3-vinyl-2,3-dihydrothiazolo[3,2-*a*]pyridinium, we suggest a BiI<sub>3</sub>-mediated cyclization of **L** accompanied by an H-shift reaction and cleavage of a CH<sub>2</sub>SPy fragment. This cleavage of a carbon–carbon bond may be facilitated by  $\pi$ -coordination of the olefinic double bond to BiI<sub>3</sub> in a reaction intermediate. The intermediacy  $\pi$ -coordinated alkene and alkyne species have also been proposed for Bi(III)-catalyzed hydration of terminal alkynes [49]. However, we have not studied in detail the mechanistic aspect of this unusual cyclization reaction. Note that BiX<sub>3</sub> salts acting as Lewis acids are well established in organic synthesis for catalytic and other Bismuth-mediated transformation [50–52]. To check the reproducibility of these findings, we also repeated the reaction using dry MeCN as a solvent. A SCXRD analysis of the resulting orange-red crystals revealed the material to be identical with that in MeOH, excluding an impact of the solvent on the outcome.

#### 4. Experimental

(*Z*)-1,4-bis(pyridine-2-ylthio)but-2-ene (**L**): 4-Mercaptopyridine (5.558 g, 50 mmol) was stirred at room temperature with an excess of potassium hydroxide in 110 mL of ethanol. A half equivalent of *cis*-1,4-dichloro-2-butene (3.125 g, 25 mmol) was added to the reaction mixture. After 1 h of stirring at room temperature, the mixture was refluxed for 3 h. After allowing it to reach ambient temperature, the resulting refrigerated product was filtered off, rinsed with a small amount of EtOH, and air-dried. After that, the solution was extracted with dichloromethane/H<sub>2</sub>O. The recombined organic layers were dried with anhydrous sodium sulfate, filtered, and then concentrated. The residual solution was purified by silica gel column chromatography using a cyclohexane/ether (4:1) mixture as eluent to yield the pure product as a yellowish liquid. The yield was 92%. Anal. Calc. for C<sub>14</sub>H<sub>14</sub>N<sub>2</sub>S<sub>2</sub> (M.W = 274.297 g·mol<sup>-1</sup>): C, 61.3; H, 5.1; N, 10.2; S, 23.3%. Found: C, 61.22; H, 5.23; N, 10.15; S, 23.39%. <sup>1</sup>H-NMR (400.1 MHz, CDCl<sub>3</sub>) at 298 K:  $\delta$  (ppm): 8.38–8.37 m, (2H<sub>d</sub>); 7.40–7.35 (m, 2H<sub>b</sub>); 7.11–7.09 (m, 2H<sub>a</sub>); 6.91–6.87 (m, H<sub>c</sub>); 5.70–5.62 (m, 2H<sub>f</sub>); 3.98–3.92 (m, 4H<sub>e</sub>). <sup>13</sup>C{<sup>1</sup>H}-NMR (100.61 MHz, CDCl<sub>3</sub>) at 298 K,  $\delta$  (ppm): 158.4 (C<sub>g</sub>); 149.3 (C<sub>d</sub>); 135.7 (C<sub>b</sub>); 128 (C<sub>f</sub>); 122.1 (C<sub>a</sub>); 119.3 (C<sub>c</sub>); 26.8 (C<sub>e</sub>).

Bis[(*Z*)-1,4-bis(pyridinium-2-ylthio)but-2-ene]Bis[3-vinyl-2,3-dihydrothiazolo[3,2-*a*]pyridinium] hexadecaiodotetrabismuthate(III) (**1**): To a stirred solution of BiI<sub>3</sub> (590 mg, 1 mmol) in methanol (15 mL), 137 mg (0.5 mmol) of the ligand **L** was added in several portions. An orange precipitate appeared rapidly. The reaction was first stirred at room temperature for 2 h, and then heated to 70 °C for 3 h. After reaching ambient temperature, the orange solid of **1** was collected by filtration, and the solvent was allowed to evaporate partially. After 4 days, orange crystals were formed and then collected by filtration. The overall yield was 82%. Anal. Calc. for C<sub>23</sub>H<sub>25</sub>Bi<sub>2</sub>I<sub>7.99</sub>N<sub>3</sub>S<sub>3</sub> (M.W = 1872.80 g·mol<sup>-1</sup>): C, 14.74; H, 1.33; N, 2.24; S, 5.13%. Found: C, 14.69; H, 1.21; N, 2.16; S, 5.24%. IR-ATR: 980–1090  $\nu$ (C-H), 1124–1156  $\delta$ (C-H<sub>arm</sub>), 1394–1468  $\delta$ (CH<sub>2</sub>), 1507–1629  $\nu$ (C=C) and  $\nu$ (C=N), 3039–3077  $\nu$ (C-H<sub>arm</sub> bonded) cm<sup>-1</sup>, 3334  $\nu$ (N-H).

Crystal data for C<sub>23</sub>H<sub>25</sub>Bi<sub>2</sub>I<sub>7.99</sub>N<sub>3</sub>S<sub>3</sub>, M = 1872.80 g·mol<sup>-1</sup>, orange crystals, crystal size 0.357 × 0.263 × 0.204 mm<sup>3</sup>, Monoclinic, space group *P*2<sub>1</sub>/*n*, a = 11.8209(6) Å, b = 18.6555(10) Å, c = 18.6908(10) Å,  $\beta$  = 97.731(2)°, V = 4084.3(4) Å<sup>3</sup>, Z = 2, D<sub>calc</sub> = 3.044 g/cm<sup>3</sup>, T = 100 K, R<sub>1</sub> = 0.0270, R<sub>w</sub> = 0.0606 for 424,002 reflections with I > = 2 $\sigma$ (I) and 12476 independent reflections. Largest diff. peak/hole e/Å<sup>-3</sup> 1.58/−1.46. Data were collected on a Bruker D8 Venture four-circle diffractometer equipped with a PHOTON II CPAD detector by Bruker AXS GmbH using graphite-monochromated MoK $\alpha$  radiation  $\lambda$  = 0.71073 Å and have been deposited at the Cambridge Crystallographic Data Centre as CCDC 2282066. (Supplementary Materials). The data can be obtained free of charge from the Cambridge Crystallographic Data Centre via <http://www.ccdc.cam.ac.uk/getstructures>, accessed on 27 December 2023. The structure was solved by direct methods and refined by full-matrix least-squares against F<sup>2</sup> (SHELXL, 2015) [53–55]. Three of the eight independent iodine positions appeared unusual when refining anisotropically. Anisotropic refinement of I<sub>2</sub>, I<sub>3</sub>,

and I8 resulted in a large nearby residual electron density very close to the initial positions of the latter. When the nearby residual electron densities peaks were included in the refinement and the occupancies of these sites (I9, I11, and I10) and the main positions (I2, I3, and I8) were refined freely, the resulting sum of the three pairs of occupancies was close to unity. This feature was taken as evidence for a split position occupied solely by iodine. We applied the occupancies of all disordered iodine atoms, which are 0.39 for I9, I10, and I11 (21) and  $-21$  for the corresponding three iodines. The final refined fractions are 0.99 for I1 and 0.61/0.39 for the following pairs: I2/I9, I3/I11, and I8/I10.

## 5. Conclusions

A novel 0-D organic–inorganic Bismuth–iodide based on a Z-Py-S(CH<sub>2</sub>CH=CHCH<sub>2</sub>)S-Py ligand was prepared and structurally characterized. We are currently extending this facile preparation of organic–inorganic hybrid materials to other BiX<sub>3</sub> salts (X = Cl and Br) and are evaluating the impact of the metal-to-ligand ratio and variation of the solvent polarity on the architecture of the resulting material.

**Supplementary Materials:** The following supporting information can be downloaded: CIF file, Check-CIF report. Figure S1. Photograph of the single crystals of compound **1**. Figure S2. IR spectrum of **L**. Figure S3. ChemDraw simulation (prediction) of the <sup>1</sup>H-NMR spectrum of **L**. Figure S4. IR spectrum of compound **1**. Scheme S1. Anionic networks, [BiI<sub>4</sub>]<sup>−</sup> and [Bi<sub>2</sub>I<sub>10</sub>]<sup>4−</sup>, derived from the parent BiI<sub>3</sub> compound illustrating the concept of dimensional reduction. Figure S5. Illustration of side contacts between one 0D tetranuclear units of Bi<sub>4</sub>I<sub>16</sub>, [C<sub>14</sub>H<sub>15</sub>S<sub>2</sub>N<sub>2</sub>]<sup>+</sup> and [C<sub>9</sub>H<sub>10</sub>SN]<sup>+</sup> cations showing H···I interactions. Figure S6. View of two adjacent 2D supramolecular networks in the 3D network. Table S1. Selected interatomic distances (Å) and angles (deg) in the crystal structure of **1**. Table S2. Hydrogen bonds geometry (Å, °) for compound **1**.

**Author Contributions:** M.E. prepared the compounds; C.S. and A.S. collected the X-ray data and solved the structure; C.H. and M.K. designed the study and analyzed the data and wrote the paper. M.E., A.K., S.A. and M.K. contributed with the conceptualization. All authors have read and agreed to the published version of the manuscript.

**Funding:** This research received no external funding.

**Data Availability Statement:** The X-ray data are deposited at CCDC as stated in the paper.

**Acknowledgments:** We thank Stéphanie Befly for recording the IR and NMR spectra.

**Conflicts of Interest:** The authors declare no conflicts of interest.

## References

1. García-Fernández, A.; Marcos-Cives, I.; Platas-Iglesias, C.; Castro-García, S.; Vázquez-García, D.; Fernández, A.; Sánchez-Andújar, M. Diimidazolium Halobismuthates [Dim]<sub>2</sub>[Bi<sub>2</sub>X<sub>10</sub>] (X = Cl<sup>−</sup>, Br<sup>−</sup>, or I<sup>−</sup>): A New Class of Thermochromic and Photoluminescent Materials. *Inorg. Chem.* **2018**, *57*, 7655–7664. [[CrossRef](#)] [[PubMed](#)]
2. Hao, P.; Wang, W.; Shen, J.; Fu, Y. Non-Transient Thermo-/Photochromism of Iodobismuthate Hybrids Directed by Solvated Metal Cations. *Dalton Trans.* **2020**, *49*, 1847–1853. [[CrossRef](#)] [[PubMed](#)]
3. Hrizi, C.; Samet, A.; Abid, Y.; Chaabouni, S.; Fliyou, M.; Koumina, A. Crystal structure, vibrational and optical properties of a new self-organized material containing iodide anions of bismuth (III), [C<sub>6</sub>H<sub>4</sub>(NH<sub>3</sub>)<sub>2</sub>]<sub>2</sub>Bi<sub>2</sub>I<sub>10</sub>·4H<sub>2</sub>O. *J. Mol. Struct.* **2011**, *992*, 96–101. [[CrossRef](#)]
4. Hrizi, C.; Trigui, A.; Abid, Y.; Chniba-boudjada, N.; Bordet, P.; Chaabouni, S.  $\alpha$ - to  $\beta$ -[C<sub>6</sub>H<sub>4</sub>(NH<sub>3</sub>)<sub>2</sub>]<sub>2</sub>Bi<sub>2</sub>I<sub>10</sub> reversible solid-state transition, thermochromic and optical studies in the p-phenylenediamine-based iodobismuthate(III) material. *J. Solid State Chem.* **2011**, *184*, 3336–3344. [[CrossRef](#)]
5. Adonin, S.A.; Sokolov, M.N.; Fedin, V.P. Polynuclear Halide Complexes of Bi(III): From Structural Diversity to the New Properties. *Coord. Chem. Rev.* **2016**, *312*, 1–21. [[CrossRef](#)]
6. Ouasri, A. Recent Advances on Structural, Thermal, Vibrational, Optical, Phase Transitions, and Catalysis Properties of Alkylendiammonium Halogenometallate Materials (Metal: Bi, Sb, Halogen: Cl, Br, I). *Rev. Inorg. Chem.* **2023**, *43*, 247–280. [[CrossRef](#)]
7. Goforth, A.M.; Tershansy, M.A.; Smith, M.D.; Peterson, L., Jr.; Kelley, J.G.; DeBenedetti, W.J.I.; zur Loye, H.-C. Structural Diversity and Thermochromic Properties of Iodobismuthate Materials Containing D-Metal Coordination Cations: Observation of a High Symmetry [Bi<sub>3</sub>I<sub>11</sub>]<sup>2−</sup> Anion and of Isolated I<sup>−</sup> Anions. *J. Am. Chem. Soc.* **2011**, *133*, 603–612. [[CrossRef](#)]

8. Ozório, M.S.; Dias, A.C.; Silveira, J.F.R.V.; Da Silva, J.L.F. Theoretical Investigation of the Role of Anion and Trivalent Cation Substitution in the Physical Properties of Lead-Free Zero-Dimensional Perovskites. *J. Phys. Chem. C* **2022**, *126*, 7245–7255. [[CrossRef](#)]
9. Heine, J. A Step Closer to the Binary: The  $1\infty[\text{Bi}_6\text{I}_{20}]^{2-}$  Anion. *Dalton Trans.* **2015**, *44*, 10069–10077. [[CrossRef](#)]
10. Feldmann, C. Preparation and Crystal Structure of  $[\text{Bi}_3\text{I}(\text{C}_4\text{H}_8\text{O}_3\text{H}_2)_2(\text{C}_4\text{H}_8\text{O}_3\text{H})_5]_2\text{Bi}_8\text{I}_{30}$  Containing the Novel Polynuclear  $[\text{Bi}_8\text{I}_{30}]^{6-}$  Anion. *J. Solid State Chem.* **2003**, *172*, 53–58. [[CrossRef](#)]
11. Hrizi, C.; Chaari, N.; Abid, Y.; Chniba-Boudjada, N.; Chaabouni, S. Structural Characterization, Vibrational and Optical Properties of a Novel One-Dimensional Organic–Inorganic Hybrid Based-Iodobismuthate(III) Material,  $[\text{C}_{10}\text{H}_7\text{NH}_3]\text{BiI}_4$ . *Polyhedron* **2012**, *46*, 41–46. [[CrossRef](#)]
12. Hamdouni, M.; Hrizi, C.; Ahmed, H.E.; Knorr, M.; Krupp, A.; Strohmman, C.; Chaabouni, S. Reaction of  $\text{Bi}(\text{NO}_3)_3$  with Quinoxaline in the Presence of HI. Synthesis of 5,6,7,8-Tetranitro-1,2,3,4-Tetrahydroquinoxaline-2,3-Diol by Serendipity: Crystal Structure, Hirshfeld and Optical Study of a Novel Energetic Compound. *J. Mol. Struct.* **2023**, *1274*, 134590. [[CrossRef](#)]
13. Louvain, N.; Mercier, N.; Boucher, F.  $\alpha$ - to  $\beta$ -(Dmes) $\text{BiI}_5$  (Dmes = Dimethyl(2-Ethylammonium)Sulfonium Dication): Umbrella Reversal of Sulfonium in the Solid State and Short I...I Interchain Contacts—Crystal Structures, Optical Properties, and Theoretical Investigations of 1D Iodobismuthates. *Inorg. Chem.* **2009**, *48*, 879–888. [[CrossRef](#)] [[PubMed](#)]
14. Saparov, B.; Mitzi, D.B. Organic–Inorganic Perovskites: Structural Versatility for Functional Materials Design. *Chem. Rev.* **2016**, *116*, 4558–4596. [[CrossRef](#)] [[PubMed](#)]
15. Ferjani, H. Structural, Hirshfeld Surface Analysis, Morphological Approach, and Spectroscopic Study of New Hybrid Iodobismuthate Containing Tetranuclear 0D Cluster  $\text{Bi}_4\text{I}_{16}\cdot 4(\text{C}_6\text{H}_9\text{N}_2)_2(\text{H}_2\text{O})$ . *Crystals* **2020**, *10*, 397. [[CrossRef](#)]
16. Chen, W.-J.; Chu, K.-B.; Song, J.-L. Low-Dimensional Bismuth(III) Iodide Hybrid Material with High Activity for the Fast Removal of Rhodamine B. *Acta Crystallogr. C* **2018**, *74*, 1744–1749. [[CrossRef](#)]
17. Pike, R.D.; Marshall, N.E.; Martucci, A.L. Alkylpyridinium Iodobismuthates(III). *J. Chem. Crystallogr.* **2022**, *52*, 161–173. [[CrossRef](#)]
18. Mahjoor, P.; Lattur, S.E. Synthesis and Structural Characterization of  $[\text{Bpyr}]_4[\text{V}_4\text{O}_4\text{Cl}_{12}]$  and  $[\text{Bpyr}]_4[\text{Bi}_4\text{Cl}_{16}]$  Grown in Ionic Liquid  $[\text{Bpyr}][\text{AlCl}_4]$  (Bpyr = 1-Butylpyridinium). *Cryst. Growth Des.* **2009**, *9*, 1385–1389. [[CrossRef](#)]
19. Rheingold, A.L.; Uhler, A.D.; Landers, A.G. Synthesis, Crystal Structure and Molecular Geometry of  $[(\text{Eta}-5-\text{C}_5\text{H}_5)_2\text{Fe}]_4[\text{Bi}_4\text{Br}_{16}]$ , the Ferrocenium Salt of a “Cluster of Octahedra” Hexadecabromotetrabismuthate Counterion. *Inorg. Chem.* **1983**, *22*, 3255–3258. [[CrossRef](#)]
20. Chen, Y.; Yang, Z.; Guo, C.-X.; Ni, C.-Y.; Ren, Z.-G.; Li, H.-X.; Lang, J.-P. Iodine-Induced Solvothermal Formation of Viologen Iodobismuthates. *Eur. J. Inorg. Chem.* **2010**, *33*, 5326–5333. [[CrossRef](#)]
21. Artem'ev, A.V.; Samsonenko, D.G. Organic-Inorganic Hybrid Iodobismuthate,  $[\text{Bi}(\text{L})_4(\text{H}_2\text{O})]\text{Bi}_3\text{I}_{12}$ , Based on Tris(2-Pyridyl)Phosphine Oxide (L): Synthesis, Structure and Air-Oxidation into  $[\text{Bi}(\text{L})_4]_2[\text{Bi}_4\text{I}_{16}(\text{I}_3)_2]$ . *Inorg. Chem. Commun.* **2018**, *93*, 47–51. [[CrossRef](#)]
22. Sharutin, V.V.; Egorova, I.V.; Levchuk, M.V.; Bukvetskii, B.V.; Popov, D.Y. Reaction of Tetraphenylantimony Bromide with O-Tolylbismuth Bis(2,5-Dimethylbenzenesulfonate). The Formation of Tetranuclear Anion  $[\text{Bi}_4\text{Br}_{16}]^{4-}$ . *Russ. J. Coord. Chem.* **2002**, *28*, 613–617. [[CrossRef](#)]
23. Genge, A.R.J.; Levason, W.; Reid, J. Bismuth(III) thioether chemistry: The synthesis and structure of  $[\text{Bi}_4\text{Cl}_{12}(\text{MeSCH}_2\text{CH}_2\text{CH}_2\text{SMe})_4]\text{n}\cdot\text{nH}_2\text{O}$ , a highly unusual network involving  $\text{Bi}_4\text{Cl}_4$  rings and bridging dithioether ligands. *Chem. Commun.* **1989**, *19*, 2159–2160. [[CrossRef](#)]
24. Clegg, W.; Norman, N.C.; Pickett, N.L. Synthesis and structure of  $[\text{SMe}_3]_2[\text{Bi}_2\text{I}_8(\text{SMe}_2)_2]$ : A dimethylsulphide complex of bismuth(III). *Polyhedron* **1993**, *12*, 1251–1252. [[CrossRef](#)]
25. Arar, W.; Khatyr, A.; Knorr, M.; Strohmman, C.; Schmidt, A. Bis( $\mu$ -iodo)-tetrakis(O-methyl N-phenylthiocarbamate)-tetraiodo-dibismuth. *Molbank* **2022**, *2022*, M1381. [[CrossRef](#)]
26. Bonnot, A.; Knorr, M.; Guyon, F.; Kubicki, M.M.; Rousselin, Y.; Strohmman, C.; Fortin, D.; Harvey, P.D. 1,4-Bis(arylthio)but-2-enes as Assembling Ligands for  $(\text{Cu}_2\text{X}_2)_n$  (X = I, Br; n = 1, 2) Coordination Polymers: Aryl Substitution, Olefin Configuration, and Halide Effects on the Dimensionality, Cluster Size, and Luminescence Properties. *Cryst. Growth Des.* **2016**, *16*, 774–788. [[CrossRef](#)]
27. Zheng, Y.; Li, J.-R.; Du, M.; Zou, R.-Q.; Bu, X.-H. Novel Silver(I) Coordination Polymers with a Series of Bis(arylthio)ether Ligands Bearing a trans-2-Butene Backbone. *Cryst. Growth Des.* **2005**, *5*, 215–222. [[CrossRef](#)]
28. Sorg, J.R.; Wehner, T.; Matthes, P.R.; Sure, R.; Grimme, S.; Heine, J.; Müller-Buschbaum, K. Bismuth as a versatile cation for luminescence in coordination polymers from  $\text{BiX}_3$  /4,4'-bipy: Understanding of photophysics by quantum chemical calculations and structural parallels to lanthanides. *Dalton Trans.* **2018**, *475*, 7669–7681. [[CrossRef](#)]
29. Yan, X.-W.; Haji-Hasani, E.; Morsali, A. Syntheses and structural characterization of two new nanostructured Bi(III) supramolecular polymers via sonochemical method. *Ultrasonics Sonochem.* **2016**, *315*, 129–134. [[CrossRef](#)]
30. Bondi, A. Van Der Waals Volumes and Radii. *J. Phys. Chem.* **1964**, *68*, 441–451. [[CrossRef](#)]
31. Tershansy, M.A.; Goforth, A.M.; Gardinier, J.R.; Smith, M.D.; Peterson, L.; zur Loye, H.-C. Solvothermal Syntheses, High- and Low-Temperature Crystal Structures, and Thermochromic Behavior of  $[1,2\text{-Diethyl-3,4,5-Trimethyl-Pyrazolium}]_4[\text{Bi}_4\text{I}_{16}]$  and  $[1,10\text{-Phenanthroline}][\text{BiI}_4]\cdot(\text{H}_2\text{O})$ . *Solid State Sci.* **2007**, *9*, 410–420. [[CrossRef](#)]
32. Goforth, A.M.; Peterson, L.; Smith, M.D.; zur Loye, H.-C. Syntheses and Crystal Structures of Several Novel Alkylammonium Iodobismuthate Materials Containing the 1,3-Bis-(4-Piperidinium)Propane Cation. *J. Solid State Chem.* **2005**, *178*, 3529–3540. [[CrossRef](#)]

33. Buikin, P.A.; Rudenko, A.Y.; Ilyukhin, A.B.; Kotov, V.Y. Synthesis and Properties of Hybrid Halobismuthates of N-Acetylpyridinium Derivatives. *Russ. J. Inorg. Chem.* **2021**, *66*, 482–489. [[CrossRef](#)]
34. Bi, W.; Mercier, N. Reversible dynamic isomerism change in the solid state, from Bi<sub>4</sub>I<sub>16</sub> clusters to BiI<sub>4</sub> 1D chains in L-cystine based hybrids: Templating effect of cations in iodobismuthate network formation. *CrystEngComm* **2008**, *44*, 5743–5745. [[CrossRef](#)]
35. Du, H.; Wang, C.; Li, Y.; Zhang, W.; Xu, M.; Li, S.; Lu, Y.; Niu, Y.; Hou, H. A supramolecular metal-organic framework derived from bismuth iodide and 4,4'-bipyridinium derivative: Synthesis, structure and efficient adsorption of dyes. *Micropor. Mesopor. Mater.* **2015**, *214*, 136–142. [[CrossRef](#)]
36. Dennington, A.J.; Weller, M.T. Synthesis, structure and optoelectronic properties of hybrid iodobismuthate & iodoantimonate semiconducting materials. *Dalton Trans.* **2018**, *47*, 3469–3484. [[CrossRef](#)]
37. Adonin, S.; Usoltsev, A.N.; Novikov, A.S.; Kolesov, B.A.; Fedin, V.P.; Sokolov, M.N. One- and Two-Dimensional Iodine-Rich Iodobismuthate(III) Complexes: Structure, Optical Properties, and Features of Halogen Bonding in the Solid State. *Inorg. Chem.* **2020**, *59*, 3290–3296. [[CrossRef](#)]
38. Yin, W.-Y.; Weng, Y.-G.; Jiang, M.; Yu, S.-K.; Zhu, Q.-Y.; Dai, J. A Series of Tetrathiafulvalene Bismuth Chlorides: Effects of Oxidation States of Cations on Structures and Electric Properties. *Inorg. Chem.* **2020**, *59*, 5161–5169. [[CrossRef](#)]
39. Ounalli, C.; Essid, M.; Bruno, G.; Santoro, A.; Abid, S.; Aloui, Z. Synthesis, Crystallographic Structure, DFT Computational Studies and Hirshfeld Surface Analysis of a New Tetranuclear Anionic Bromobismuthate(III): [C<sub>12</sub>H<sub>20</sub>N<sub>2</sub>]<sub>2</sub>Bi<sub>4</sub>Br<sub>16</sub>·2H<sub>2</sub>O. *J. Mol. Struct.* **2021**, *1243*, 130916. [[CrossRef](#)]
40. Vasiliev, A.A.; Bykov, A.V.; Shestimerova, T.A.; Bykov, M.A.; Goncharenko, V.E.; Shevelkov, A.V. Supramolecular Structures of New Tetranuclear Hydroxypiperidine Iodoantimonates(III). *Russ. Chem. Bull.* **2023**, *72*, 641–650. [[CrossRef](#)]
41. Mercier, N.; Louvain, N.; Bi, W. Structural diversity and retro-crystal engineering analysis of iodometalate hybrids. *CrystEngComm* **2009**, *11*, 720–734. [[CrossRef](#)]
42. Bozorth, R.M. The crystal structure of cadmium iodide. *J. Am. Chem. Soc.* **1922**, *44*, 2232. [[CrossRef](#)]
43. Shannon, R.D. Revised Effective Ionic Radii and Systematic Studies of Interatomic Distances in Halides and Chalcogenides. *Acta Crystallogr. A* **1976**, *32*, 751–767. [[CrossRef](#)]
44. Van Bolhuis, F.; Koster, P.B.; Migchelsen, T. Refinement of the Crystal Structure of Iodine at 110° K. *Acta Crystallogr.* **1967**, *23*, 90–91. [[CrossRef](#)]
45. Turner, M.J.; McKinnon, J.J.; Wolff, S.K.; Grimwood, D.J.; Spackman, P.R.; Jayatilaka, D.; Spackman, M.A. University of Western Australia. 2017. Available online: <https://crystalexplorer.scb.uwa.edu.au/> (accessed on 1 June 2022).
46. Spackman, M.A.; Jayatilaka, D. Hirshfeld surface analysis. *CrystEngComm* **2009**, *11*, 19–32. [[CrossRef](#)]
47. Charmant, J.P.H.; Norman, N.C.; Orpen, A.G.; Starbuck, J. 4,4'-Bipyridyl adduct of an iodobismuthate anion linked by a 4,4'-bipyridinium cation. *Acta Crystallogr.* **2003**, *E59*, m1000–m1001. [[CrossRef](#)]
48. Potapova, V.A.; Ishigeev, R.S.; Shkurchenko, I.V.; Amosova, S.V. Assembling of Thiazolo [3,2-a]pyridinium Salts via the Reaction of 2-Pyridinesulfonyl Halides with Vinyl Ethyl Ether. *Russ. J. Gen. Chem.* **2019**, *89*, 2601–2603. [[CrossRef](#)]
49. Otvos, S.B.; Szecsenyi, Z.; Ferenc Fulop, F. Bismuth(III)-Catalyzed Hydration of Terminal Alkynes: Sustainable Synthesis of Methyl Ketones in Batch and Flow. *ACS Sustain. Chem. Eng.* **2019**, *7*, 13286–13293. [[CrossRef](#)]
50. Ollevier, T. (Ed.) *Bismuth-Mediated Organic Reactions*; Springer: Berlin/Heidelberg, Germany, 2012; pp. 69–142, 179–198.
51. Salvador, J.A.R.; Pinto, R.M.A.; Silvestre, S.M. Recent advances of bismuth(III) salts in organic chemistry: Application to the synthesis of heterocycles of pharmaceutical interest. *Curr. Org. Synth.* **2009**, *6*, 426–470. [[CrossRef](#)]
52. Ollevier, T. New trends in bismuth-catalyzed synthetic transformations. *Org. Biomol. Chem.* **2013**, *11*, 2740–2755. [[CrossRef](#)]
53. Sheldrick, G. SHELXT—Integrated space-group and crystal-structure determination. *Acta Crystallogr. A* **2015**, *71*, 3–8. [[CrossRef](#)] [[PubMed](#)]
54. Sheldrick, G. Crystal structure refinement with SHELXL. *Acta Crystallogr. C* **2015**, *71*, 3–8. [[CrossRef](#)] [[PubMed](#)]
55. Dolomanov, O.V.; Bourhis, L.J.; Gildea, R.J.; Howard, J.A.; Puschmann, H. OLEX2: A complete structure solution, refinement and analysis program. *J. Appl. Crystallogr.* **2009**, *42*, 339–341. [[CrossRef](#)]

**Disclaimer/Publisher's Note:** The statements, opinions and data contained in all publications are solely those of the individual author(s) and contributor(s) and not of MDPI and/or the editor(s). MDPI and/or the editor(s) disclaim responsibility for any injury to people or property resulting from any ideas, methods, instructions or products referred to in the content.